Tracing the fate of seabird-derived nitrogen in a coral reef using nitrate and coral skeleton nitrogen isotopes

Noémie Choisnard [1,2]* Nicolas Noel Duprey [1]* Tanja Wald [1] Martin Thibault [3,4]
Fanny Houlbrèque [3] Alan D. Foreman [1] Pascale Cuet [5] Mireille M. M. Guillaume [6,7]
Hubert Vonhof [1] Daniel M. Sigman [8] Gerald H. Haug [1] Jean-François Maguer [9]
Stéphane L'Helguen [9] Alfredo Martínez-García [1] Anne Lorrain [9]

[1]Max Planck Institute for Chemistry (Otto Hahn Institute), Mainz, Germany
[2]Department of Biological Oceanography, Leibniz Institute for Baltic Sea Research Warnemünde, Rostock, Germany
[3]UMR ENTROPIE (IRD—Université de La Réunion—CNRS—Université de la Nouvelle Calédonie—Ifremer), Laboratoire
d'Excellence Labex-CORAIL, Institut de Recherche Pour le Développement, Nouméa Cedex, New Caledonia
[4]Centre d'Ecologie et des Sciences de la Conservation (CESCO), Museum National d'Histoire Naturelle, Station de Biologie
Marine, Concarneau, France
[5]UMR ENTROPIE (Université de La Réunion—IRD—CNRS—Université de la Nouvelle Calédonie—Ifremer), Laboratoire
d'Excellence Labex-CORAIL, St Denis Cedex 09, La Réunion, France
[6]Departement of Aviv, UMR BOrEA Muséum National d'Histoire Naturelle–SU–CNRS–IRD–UCN–UA, Paris, France
[7]LabEx CORAIL, Perpignan, France
[8]Department of Geosciences, Princeton University, Princeton, New Jersey, USA
[9]University of Brest, CNRS, IRD, Ifremer, LEMAR, Plouzané, France

Abstract

Seabirds transfer nutrients from the ocean to their nesting island, potentially altering nitrogen (N) cycling within adjacent terrestrial and marine ecosystems. Yet, the processes involved in seabird-N transfer along the land–sea continuum remain elusive. Using $\delta^{15}N$ and $\delta^{18}O$ measurements of groundwater nitrate, we demonstrate the role of brackish groundwater located within a coral island's landmass as a major reservoir of nitrate (at millimolar levels). Nearly all of the total dissolved seabird-derived N leaching into the groundwater (mostly ammonium and uric acid) is converted to nitrate by nitrification, as supported by the relatively low $\delta^{18}O$ of the groundwater nitrate (3.97‰ ± 0.30‰). Comparison of nitrate $\delta^{15}N$ and $\delta^{18}O$ suggests that little denitrification takes place within the groundwater lens, implying that the high $\delta^{15}N$ of groundwater nitrate (13.73‰ ± 0.05‰) derives from the high trophic position of seabirds and postdepositional processes that increase the $\delta^{15}N$ of seabird excreta. Seawater and coral skeleton samples from a reef flat exposed to groundwater had higher $\delta^{15}N$ values than at sites devoid of groundwater influence, indicating that the main source of N at the latter site was the Subtropical Upper Water, while the groundwater nitrate dominated the exposed reef flat N pool up to 200 m from shore. In addition, these results indicate that coral-bound $\delta^{15}N$ can detect seabird-derived nitrate $\delta^{15}N$, raising opportunities to reconstruct historical seabird-N inputs to coral reefs in relation to climatic and other changes, such as the introduction of invasive species.

*Correspondence: noemie.choisnard@io-warnemuende.de; n.duprey@mpic.de

Additional Supporting Information may be found in the online version of this article.

Noémie Choisnard and Nicolas Noel Duprey contributed equally to this work and share first authorship.
Alfredo Martínez-García and Anne Lorrain share senior/last authorship.
Author Contribution Statement: Duprey NN, Houlbrèque F, Thibaut M and Lorrain A conceived and designed the research. All authors contributed to the collection and compilation of data. Choisnard N, Duprey NN, Thibaut M Lorrain A and Wald T analyzed the data. Choisnard N, Duprey NN, Thibaut M and Lorrain A wrote the manuscript. All authors contributed to content revisions and approved the final text.

Nutrient transfer across ecosystem boundaries is a major determinant of habitat dynamics, structure, and productivity (Anderson and Polis 1998, 1999). In oligotrophic regions of the ocean, small and isolated ecosystems such as tropical islands are particularly dependent on exogenous nutrients (Polis et al. 1997) provided by various animal vectors. In many cases, massive seabird colonies dominate the nutrient fluxes to islands, conveying nutrients from the open ocean, where they feed, to their breeding grounds (Anderson and Polis 1998) in form of seabird feces (guano) that are enriched in nitrogen (N) and phosphorus (P) relative to other elements (Staunton Smith and Johnson 1995).

At the larger scale, seabird-derived N inputs are estimated to be 591 Gg N yr^{-1}, similar in magnitude to the global groundwater inputs to the ocean (Otero et al. 2018). In the vicinity of tropical seabird nesting islands and within 400 m from shore, guano-derived N has been found to be a major N source for coral reefs (Lorrain et al. 2017; Benkwitt et al. 2021), as the amount of dissolved inorganic N in these reefs can be about 90-fold higher than the amount of other N sources for corals, such as zooplankton (Wiedenmann et al. 2023). These inputs have also been shown to boost reef productivity and thus ecosystem function (Dubinsky and Berman-Frank 2001; Graham et al. 2018) as well as to increase the abundance of crustose coralline algae and herbivorous fishes following a bleaching event (Benkwitt et al. 2019). Yet, one of the most spectacular effects of seabird-derived N is the modulation of the feeding strategy of mixotrophic corals, increasing the assimilation of inorganic N sources (Thibault et al. 2022) and the fourfold increase in the growth rate of corals exposed to guano-N (Savage 2019).

However, anthropogenic excess N relative to other nutrients has also proved to be detrimental to coral reefs, depending on the N form considered (Duprey et al. 2016; Burkepile et al. 2020). In particular, significant increases in inorganic N supply can cause an imbalance in the coral-Symbiodiniaceae symbiosis, curtailing carbon translocation to the coral (Dubinsky and Berman-Frank 2001) and increasing its sensitivity to extreme warming events via bleaching (Wiedenmann et al. 2013). Changes in the supply of nutrients can therefore act as a stress or a beneficial factor on coral communities (Fabricius et al. 2013; DeCarlo et al. 2020). Constraining the mechanisms controlling the seabird-N supply, and the magnitude of its spatiotemporal variability is, therefore, key to understanding abutting coral reef functioning and improving the conservation of these ecosystems.

While it is clear that N transfer on seabird nesting islands is driven by guano deposition, the processes by which N reaches reefs remain uncertain. The direct dropping of feces in the water surrounding such islands has been hypothesized to be an important pathway for seabird-derived N, as dissolution experiments have shown that about 90% of the N from guano is released in solution as NH_4^+ within minutes (Loder et al. 1996). Guano deposition onto the island is also thought to play a major role in N transfer to the reef via several pathways. Under moist conditions, degradation of guano through bacterial hydrolysis generates NH_4^+, which deprotonates and volatilizes to the atmosphere as ammonia (NH_3) (Wright 1995; Blackall et al. 2008). This NH_3 is mostly transported away from the colony by winds before returning to the oceans via deposition or as part of air/sea equilibration (Altieri et al. 2014). In contrast, under very dry or wet conditions, NH_3 volatilization is attenuated and NH_4^+ is likely converted to nitrate (NO_3^-), which could be lost via denitrification (the reduction of NO_3^- to N_2) in case of low soil oxygen availability (Houlton et al. 2006). Otherwise, NH_4^+ and NO_3^- accumulate temporarily in the soil until they are taken up by plants, are transferred to the lagoon by runoff, or leach into the groundwater following rainfall, presenting additional routes for the transfer of seabird-derived N to the reef (Staunton Smith and Johnson 1995).

Given the spatial and temporal variability of climatic conditions, the geology of the island sites, and the fluctuations of seabird population, identifying the transfer pathways and transformations of seabird-derived N species along the various land–sea–atmosphere boundaries is challenging. One avenue by which progress in clarifying these mechanisms can be made is by monitoring changes in N isotopes in the environment. The relative abundance of ^{15}N relative to ^{14}N (expressed as $\delta^{15}N = [(^{15}N/^{14}N)_{sample}/(^{15}N/^{14}N)_{air} - 1] * 1000]$) has been used widely to identify N sources with contrasted $\delta^{15}N$ fingerprints in ecosystems (Fry 2006). For instance, seabird excreta has typically elevated $\delta^{15}N$ values (7‰ to 18.3‰ ± 1.3‰, Lorrain et al. 2017; Thibault et al. 2022) due to the seabirds' high trophic position (Anderson and Polis 1999), while the pycnocline NO_3^- has a mean $\delta^{15}N$ of 6.25‰ (Fripiat et al. 2021), and N originating from dinitrogen fixation is relatively low (~ -2‰ to 0‰, Carpenter et al. 1997). In addition, the combined analysis of N and oxygen (O) isotopes of NO_3^- allows us to identify NO_3^--consuming processes that discriminate differentially between the stable isotopes of N and O. While N and O isotopes are closely coupled during assimilation and denitrification (Granger et al. 2004, 2008), they become decoupled during nitrification (Sigman et al. 2005; Wankel et al. 2007). Furthermore, measurements of the N isotopic composition of coral skeleton-bound organic matter (CS-$\delta^{15}N$) have been used to study the evolution of the coral reef N sources over time (Muscatine et al. 2005; Wang et al. 2018; Murray et al. 2019).

Building upon this experience, we used a comprehensive sampling strategy and measured the N and O isotopic composition of NO_3^- in groundwater, offshore water, and reef flat water along a shore-ocean transect of a remote Coral Sea atoll in the Southwest Pacific (Surprise Island) that hosts up to 14,000 nesting seabird pairs. We also explore further the potential of massive coral *Porites* CS-$\delta^{15}N$ to trace the supply of seabird-derived N to the reef. We pursue three main objectives in this study: (i) characterize the different sources of N present in the coral reef ecosystem, (ii) address the pathways and transformation of seabird-derived N along the land–sea

continuum, and (iii) assess whether seabird-derived N inputs are recorded in massive *Porites* CS-δ^{15}N.

Materials and methods

Study site

D'Entrecasteaux Reef (223 km north of New Caledonia) is composed of two uninhabited atolls, Huon and Surprise (Fig. 1). Surprise Island, located on the eponymous atoll, is a 24-ha circular island culminating at 9 m above sea level. This area experiences two distinct seasons: a warm and rainy season from December to March, and a cooler and dryer season from July to October. Surprise Atoll's coral reefs host benthic coral assemblages dominated by scleractinian species (Wantiez et al. 2022). Covered with bushes and small trees, Surprise Island is a refuge for about 13 breeding marine seabird species accounting for more than 14,000 breeding pairs of epigeous species (Supporting Information Table S1; Thibault et al. 2022; Philippe-Lesaffre et al. 2023). The surrounding seawater has low nutrient concentrations (< 0.5 μM of NO_3^-), typical of the oligotrophic waters of the Coral Sea (Bonnet et al. 2015).

Sea surface salinity and tide measurement

Submarine groundwater discharge can be modulated by tidal pumping and is characterized by a drop in salinity of coastal waters during peak discharge. Because the tidal system is poorly resolved at the study site, we deployed four salinity and depth recorders (YSI OMS 600 data loggers) across the reef flat at 25, 50, 100, and 200 m from shore during the entire duration of our stay on the island (one measurement every 10 min with an accuracy of 0.1 of salinity and 0.02 m for depth, 6 d, from 04 July 2019 to 09 July 2019). This record of the tidal regime provides key information with regard to the hydrographic setting at the time of each seawater sample collection. A composite salinity anomaly time series was calculated by standardizing all individual data loggers to their own maximum salinity value (i.e., average of high tide values). This composite salinity anomaly is then independent of the maximum salinity at the different stations, with greater anomalies indicating greater salinity drop. The salinity of groundwater was measured directly using a salinity probe (YSI OMS 600).

Water sampling and analysis

Samples were collected during the cruise IGUANE 2019 aboard R/V Alis. Seawater samples (40 mL) were retrieved with a Niskin sampler in triplicate along a depth profile (at 10, 100, 200, 300, 400, and 500 m; $n = 3$ per depth) offshore Surprise Atoll, away from land influence (18.593°S, 163.070°E, Fig. 1b). Salinity, temperature, and fluorescence were obtained from a CTD probe (CTD SBE 19) mounted with a fluorescence probe in parallel to the depth profile sampling. From the temperature and salinity profiles, we calculated the seawater density to further estimate the vertical buoyancy gradient (or the square of the buoyancy frequency), (N^2) following Eq. 1 (McDougall 1987):

$$N^2 = -\frac{g}{\rho} \times \frac{\partial \rho}{\partial z} \tag{1}$$

where g is the gravity constant, ρ is the density of seawater, and z is the depth. The depth where a maximum N^2 occurred was defined as the mixed layer depth (MLD).

Seawater samples were collected on the reef flat of Surprise Island, exposed to seabird N following a transect perpendicular to the shoreline at 10, 25, 50, 100, 200, and 400 m from the shoreline at high tide (Fig. 1d). Sampling along the reef flat transect was conducted on 06 July 2019 and repeated on 09 July 2019 to assess the short-term temporal variability of the reef water properties. Groundwater samples were also collected at Surprise Island through a 2.9-m-deep borehole dug during the expedition (18.479°S, 163.086°E, Fig. 1d). The top of the water table was found 2.6 m below the surface and groundwater was pumped out using a compressed air virgin polytetrafluorethylene pump on 07 July 2019 and 09 July 2019.

As a comparison for this study, we include groundwater samples collected in April 2019 from two other tropical coral islands from the Western Indian Ocean visited on the occasion of the Climate Eparses and CLIM-EPARSE programs, to investigate the influence of different nesting seabird density on groundwater properties. Of particular interest for comparison, we present data from the groundwater of Tromelin Island, a seabird nesting island with seven times less breeding pairs than Surprise Island (Supporting Information Table S1). Groundwater was collected at an existing well located at 15.890°S, 54.520°E. We also include data from Grande Glorieuse Island, where no significant nesting seabird population can be found today due to the presence of invasive rats that decimated the seabird population (Russell and Le Corre 2009). The groundwater was sampled at an observation well located at 11.580°S, 47.300°E. To compare the influence of nesting seabird population on each island's groundwater, we calculated the bird density by dividing the number of breeding pairs by the area (resulting in 47, 2, and 0 breeding pairs per square meter for Surprise, Tromelin, and Grande Glorieuse, respectively; Supporting Information Table S1).

Nutrient concentration analysis

NO_3^- and nitrite (NO_2^-) analyses were made at the Max Planck Institute for Chemistry (MPIC), Mainz. All water samples were frozen upon collection and kept frozen until analysis. NO_x concentrations ($NO_3^- + NO_2^-$) were first determined according to Braman and Hendrix (1989) on a Teledyne API T200 NO_x analyzer with a detection limit of 0.01 μM and a precision of 0.5%. NO_2^- concentrations were determined on a continuous flow autoanalyzer (Quaatro, Seal analytical) with a detection limit of 0.01 μM. Because NO_2^- concentrations were below the detection limit in all samples, NO_x concentration is further considered as NO_3^- concentration. The NO_3^- concentrations obtained were used to calculate the volume of
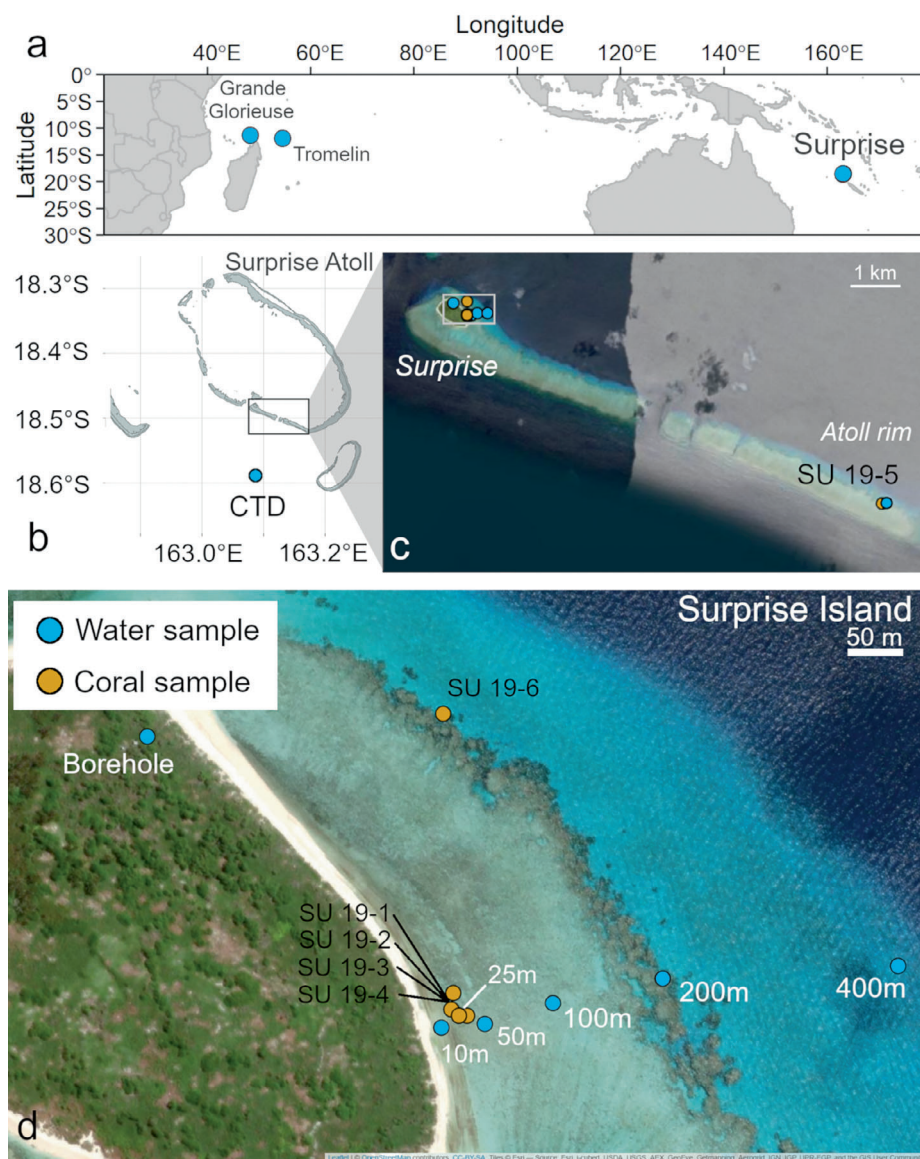
Fig. 1. Tropical seabird-nesting islands are ideally suited to study the transfer of nutrients along the land–ocean continuum. This study focuses on Surprise Island, Tromelin Island and Grande Glorieuse Island (**a**). Surprise Island, located in D′ Entrecasteaux Reef, is the main study site of this study (**b–d**). On this site, water was sampled along a shore-ocean transect (blue points in **d** at 10, 25, 50, 100, 200, and 400 m from shore) and in the groundwater body (borehole). The water column was also sampled every 100 m between 10 and 500 m depth at an oceanic site where a conductivity, temperature, and depth probe was deployed (CTD, 18.593°S, 163.070°E, **b**). Six coral cores were retrieved (yellow points, **c**, **d**). Four were collected at approximately 25 m offshore at the surface at the island site (SU19-1, SU19-2, SU19-3, SU19-4), one roughly 200 m offshore the island at 5 m depth (SU19-6) and one is the atoll rim site, at approximately 7 m depth (SU19-5, **c**). The atoll rim site was referred to as a "reference site" in previous studies of the region (e.g., Thibault et al. 2022). The map was generated using the WCMC008_CoralReef2018 and the ESRI World Imagery data files.

sample to be injected to achieve a consistent N-content for δ^{15}N- and $\delta^{18}O - (NO_3^- + NO_2^-)$ analysis described further. The NO_3^- concentration values reported in this study were obtained during the NO_3^- isotope analyzes to take full advantage of the mass spectrometer's sensitivity (*see* section below). NH_4^+ concentrations were measured onboard using a Turner Trilogy fluorometer according to Holmes et al. (1999), with a detection limit of $0.05\,\mu M$, and urea concentrations were

measured at the LEMAR, Brest, with a precision of $\pm 0.04\,\mu M\,N$ (Aminot and Kerouel 1982).

Dual isotope (δ^{15}N, δ^{18}O) analysis of $(NO_3^- + NO_2^-)$ and NO_3^-

The δ^{15}N and δ^{18}O of $(NO_3^- + NO_2^-)$ were measured in duplicate using the denitrifier method (Sigman et al. 2001; Casciotti et al. 2002) at the Martínez-García Laboratory, MPIC, following the protocols of Weigand et al. (2016). Then, 5–

10 nmol of $(NO_3^- + NO_2^-)$ were quantitatively converted to nitrous oxide (N_2O) gas by a strain of denitrifying bacteria (*Pseudomonas chlororaphis* subsp. *aureofaciens*) that lacks an active N_2O reductase enzyme. The resulting N_2O was analyzed for stable N and O isotopic composition using a custom-made N_2O extraction and purification system coupled to a MAT253 stable isotope ratio mass spectrometer (McIlvin and Casciotti [2011]; Weigand et al. [2016]).

NO_2^- can affect measurements of $\delta^{18}O - NO_3^- + NO_2^-$ even at undetectable NO_2^- concentration. In fact, NO_2^- is subject to a smaller loss of O atoms than NO_3^- during bacterial reduction to N_2O, leading to O isotopic composition approximately 25‰ lower than that of N_2O generated from NO_3^- with the same initial $\delta^{18}O$ (Casciotti et al. [2007]). In order to measure the $\delta^{15}N$ and $\delta^{18}O$ of NO_3^-, all samples were also treated with sulfamic acid to remove NO_2^- prior to bacterial conversion to N_2O, according to the protocol of Granger and Sigman ([2009]).

We adjusted the method for the measurement of the isotopic composition of $(NO_3^- + NO_2^-)$ and NO_3^- of waters with low NO_3^- content ($< 2\,\mu M$), by injecting larger volumes of samples (up to 5 mL). Using large volumes usually leads to isotopic offsets, in part because of incomplete recovery of the N_2O formed (Zhou et al. [2022]). As these offsets are larger for $\delta^{18}O$ at NO_3^- concentrations below $0.1\,\mu M$, only samples above this threshold were run for $\delta^{18}O$ analysis. In order to correct potential bias induced by volume effects on our isotope ratio analyses, sets of NO_3^- standards (IAEA-NO_3 and USGS34) emulating our sample concentrations (and volumes) were measured every 10 samples (3–4 times per run). These standards were used for calibration and bacteria blank correction, with an uncertainty of less than 0.08‰ and 0.13‰ for $\delta^{15}N$ and $\delta^{18}O$ (1 SD), respectively. In-house standards (MSM) were used for later data correction and long-term reproducibility, indicating a precision $< 0.06‰$ for $\delta^{15}N$ and 0.17‰ for $\delta^{18}O$ ($n = 27$). $\delta^{15}N$ and $\delta^{18}O$ values are reported on the AIR and V-SMOW scales, respectively.

Water $\delta^{18}O$ analysis

$\delta^{18}O$-H_2O was measured at the Vonhof Laboratory (MPIC), to better describe our study sites and characterize potential sources of O atoms for NO_3^- during nitrification. Each sample was analyzed on a Thermo Delta V mass spectrometer equipped with a GASBENCH II preparation device and autosampler. In brief, 0.5 mL of water was injected through the septum cap of a 12-mL exetainer vial (pre-flushed with a mixture of helium—He—and 0.3% of carbon dioxide, CO_2). Subsequently, samples were left for 24 h at 21°C to enable the equilibration of the O isotope composition of the headspace CO_2 with the water sample. After that time, the headspace CO_2 of each sample was transferred to the GASBENCH II unit using He as a carrier gas, where trace amounts of water vapor and N gas were removed prior analysis with the mass spectrometer. Data are reported as $\delta^{18}O$ values on the V-SMOW scale. Two in-house water standards KONA2019 and MainzTap2019, calibrated to

the V-SMOW2–SLAP2 scale, have $\delta^{18}O$ values of 0.16‰ and −8.70‰ respectively. The reproducibility of both in-house standards was better than 0.1‰ (1 SD) for $\delta^{18}O$ over the entire dataset.

Particulate organic matter $\delta^{15}N$

Samples for particulate organic N (PN) were taken along the transect and at the atoll rim, by filtering 2–4 L of seawater onto pre combusted 25-mm GF/F filters (Whatman, nominal porosity: 0.7 μm). Filters were dried at 60°C before being wrapped in tin cups prior analysis on a Thermo Delta Advantage mass spectrometer in continuous flow mode connected to a Costech Elemental Analyzer via a ConFlo IV at Union College (Schenectady, NY). Reference standards (sorghum flour, acetanilide, ammonium sulfate [IAEA-N-2] and caffeine [IAEA-600]) were used for isotopic corrections, and to assign the data to the appropriate isotopic scale. The combined analytical uncertainty for $\delta^{15}N$ (Air) is $\pm$ 0.18‰, based on seven Acetanilide standards over two analytical sessions.

Coral coring and processing

Six coral cores (diameter: 4 cm) were drilled from massive *Porites* sp. colonies (< 60 cm diameter) to reconstruct the spatial variability of guano inputs across the land–sea continuum by measurement of $\delta^{15}N$ in the skeletal organic matrix (CS-$\delta^{15}N$). Core SU 19–5 (length: 57 cm) was collected at 7 m depth on the inner section of the atoll rim (Fig. [1d]) and is considered as the reference for corals away from seabird influence. Cores SU 19-1 to SU 19-4 (length: 21–41.5 cm) were collected on the reef flat within 25–50 m from the shore, at 2–3 m depth (Fig. [1]), where elevated $\delta^{15}N$ values have been previously reported for benthic organisms (coral, macroalgae) due to seabird-derived N supply (Lorrain et al. [2017]; Thibault et al. [2022]). Core SU 19-6 (length: 57 cm) was collected at the island site, approximately 200 m offshore and at 5 m depth, to assess the variability of N sources along the reef flat. Each core was cut into 8-mm-thick slabs using a diamond-coated blade mounted on a rock saw. Skeleton samples were taken within the first 5 mm below the tissue layer of each core using a hand-held drill, a zone likely to correspond to the last year of growth (sample volume: $\sim 5 * 5 * 2$ mm^3). Each powdered sample (approximately 30 mg) was sieved and separated into fractions > 63 and < 250 μm to facilitate the weighing and the cleaning procedure described below.

Coral skeleton $\delta^{15}N$ analysis

Coral skeleton $\delta^{15}N$ analysis was performed in the Martínez-García Laboratory at the MPIC. Aliquots (8 mg) of the > 63 μm sample fraction were oxidatively cleaned using (13%) reagent grade sodium hypochlorite for 24 h and were rinsed three times with MQ water. The coral skeleton was decalcified using ultrapure 4 N HCl, and the remaining organic matrix was oxidized into NO_3^- using four times recrystallized potassium persulfate (Wang et al. [2015]; Moretti et al. [2023]).

The NO_3^- obtained was subsequently converted into N_2O by denitrifying bacteria, and the resulting N_2O was analyzed for stable N isotopic composition using the extraction and purification system described in Weigand et al. (2016). International amino acid standards (USGS40 and USGS41) and NO_3 standards (IAEA-NO-3 and USGS44) were used for blank correction and calibration, and two in-house coral standards were used to monitor reproducibility: MPIC-Lo-1 and MPIC-Po-1 (Moretti et al. 2023; Martínez-García et al. 2022). The analytical precision calculated over 17 analyses of each coral standard was less than 0.2‰ (1 SD) and was the value reported on figures when no replicate measurements were available.

Mixing model of N-sources contributions to the reef-flat $\delta^{15}N - (NO_3^- + NO_2^-)$

The influence of different sources on seawater $\delta^{15}N - (NO_3^- + NO_2^-)$ was computed using a simple mixing model (Fry 2006), adapted to take into account the different N-sources to the reef. Because of the strong currents and wind
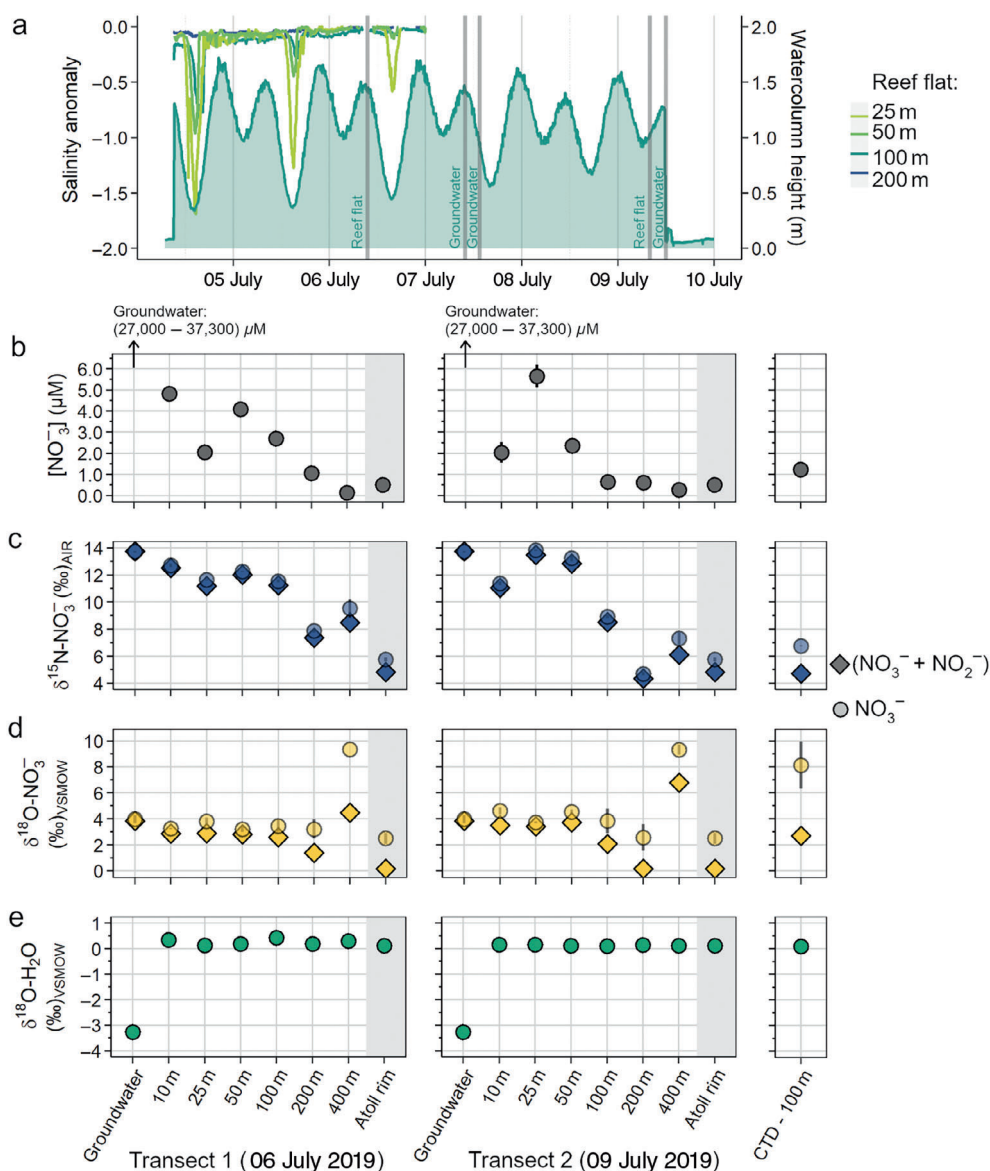

Fig. 2. The seawater properties across the reef flat of Surprise Island informs about the processes and the footprint of the seabird-derived N across the land-sea continuum. The variation of the water column depth (m) and salinity anomaly on the reef flat (**a**) put into light the impact of tide on the reef flat. To capture its forcing on (**b**) NO_3^- concentration, (**c**) $\delta^{15}N - NO_3^-$, and (**d**) $\delta^{18}O - NO_3^-$ and (**e**) $\delta^{18}O - H_2O$ across the reef flat, the transect was sampled on two separate occasions; transect 1 (06 July) corresponding to high tide and transect 2 (09 July) corresponding to low tide. Distance is measured from the high water mark. Diamond symbols represent $(NO_3^- + NO_2^-)$ data and circle symbols NO_3^--only data. The colored lines in the first panel account for the distance from shore and gray bars indicate the sampling dates. For nutrients and isotopic analysis, two duplicates have been analyzed.

stress in the region (Kessler and Cravatte 2013), we made the assumption that the reef flat exposed to seabird-derived N was also exposed to the same water mass as the one sampled at the CTD site (Fig. 1b). The validity of this hypothesis was confirmed by looking at the similarities between the isotopic composition of the water sampled at the CTD site and the one sampled at the most distal location from shore along the reef transect (*see* Discussion).

We applied our mixing model to quantify $f_{groundwater}$ and f_{ocean}, the proportion of groundwater and oceanic water, respectively, explaining the reef flat $\delta^{15}N - NO_3^-$:

$$f_{groundwater} = \frac{\delta^{15}N_{reef} - \delta^{15}N_{ocean}}{\delta^{15}N_{groundwater} - \delta^{15}N_{ocean}} \quad (2)$$

$$f_{ocean} = 1 - f_{groundwater} \quad (3)$$

where $\delta^{15}N_{reef}$ is the $\delta^{15}N - (NO_3^- + NO_2^-)$ observed along the land–sea continuum and $\delta^{15}N_{ocean}$ is the shallowest $\delta^{15}N - (NO_3^- + NO_2^-)$ measured, in this case, observed at 100 m depth on the CTD profile.

Results

Tidal forcing of near-shore waters

Tides at the study site were composed of both semidiurnal and diurnal oscillations (Fig. 2a). At a distance of 100 m offshore, the semidiurnal tides showed an amplitude of 0.6 m while the diurnal oscillation presented a range of 1.5 m (Fig. 2a). These latter oscillations, covering three tidal cycles, were accompanied by a salinity decrease at low tide, which was greater 25 m from shore (− 1.7) than 100 m offshore (− 0.7), and which was nonexistent at 200 m from the island (Fig. 2a).

NO_3^- characteristics of oceanic, reef flat, and ground waters

For the sake of completeness, we analyzed both $\delta^{15}N$- and $\delta^{18}O - (NO_3^- + NO_2^-)$ and $\delta^{15}N$- and $\delta^{18}O - NO_3^-$ to account for the potential influence of NO_2^- in the N isotope ratio, as this N form may be influenced by strong fractionation. Comparing the $\delta^{15}N - NO_3^-$ and $\delta^{15}N - (NO_3^- + NO_2^-)$ datasets thus provides additional details about the N-cycling pathways which may change the isotopic composition of NO_2^- relative to NO_3^- (Casciotti et al. 2007; Kemeny et al. 2016), as observed in the
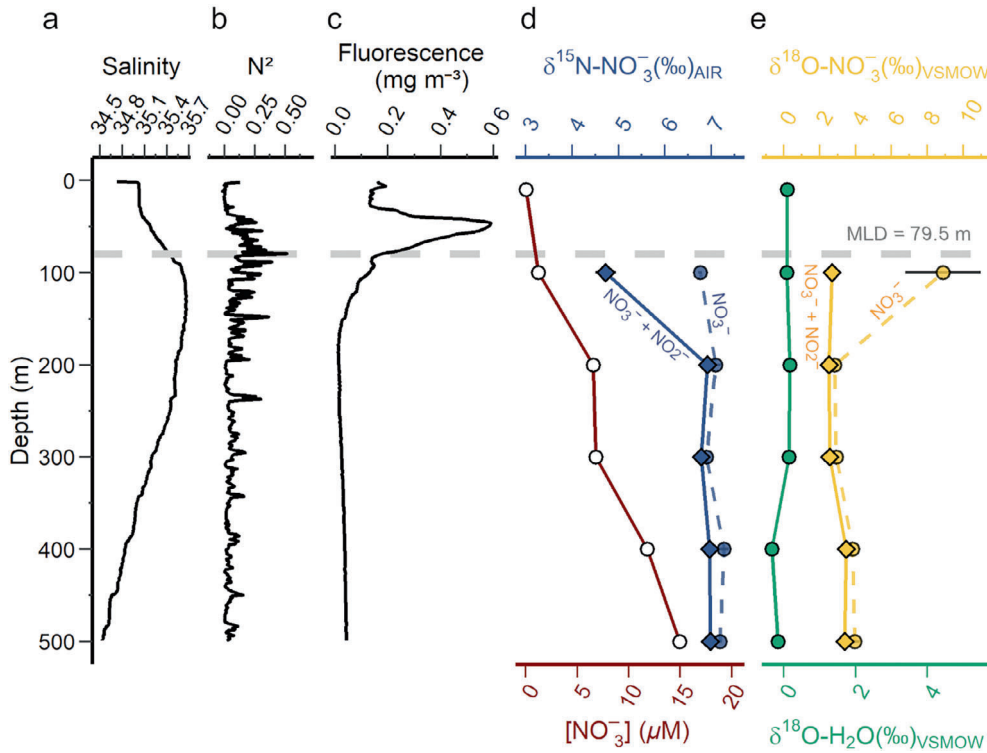

Fig. 3. The water column properties offshore Surprise Island (western Pacific) provide important information about the sources and the processes controlling the N cycle in the Coral Sea. Depth profiles of salinity and buoyancy frequency (N^2) and fluorescence were collected at our oceanic site (*see* CTD in Fig. 1b) to establish the biological and physical settings near the island (**a–c**). NO_3^- concentration [NO_3^-] (red line, empty circles, **d**) and $\delta^{15}N - NO_3^-$ (dark blue and dashed lines, **d**) as well as $\delta^{18}O - NO_3^-$ (yellow and dashed lines, **e**) and $\delta^{18}O$-H$_2$O (green, **e**) were measured to unveil the dominant N-cycle processes. Isotopic compositions obtained before NO_2^- removal [$\delta^{15}N$- and $\delta^{18}O - (NO_3^- + NO_2^-)$] are represented by the diamond symbols. The horizontal gray dashed line represents the MLD estimated from the buoyancy frequency profile.
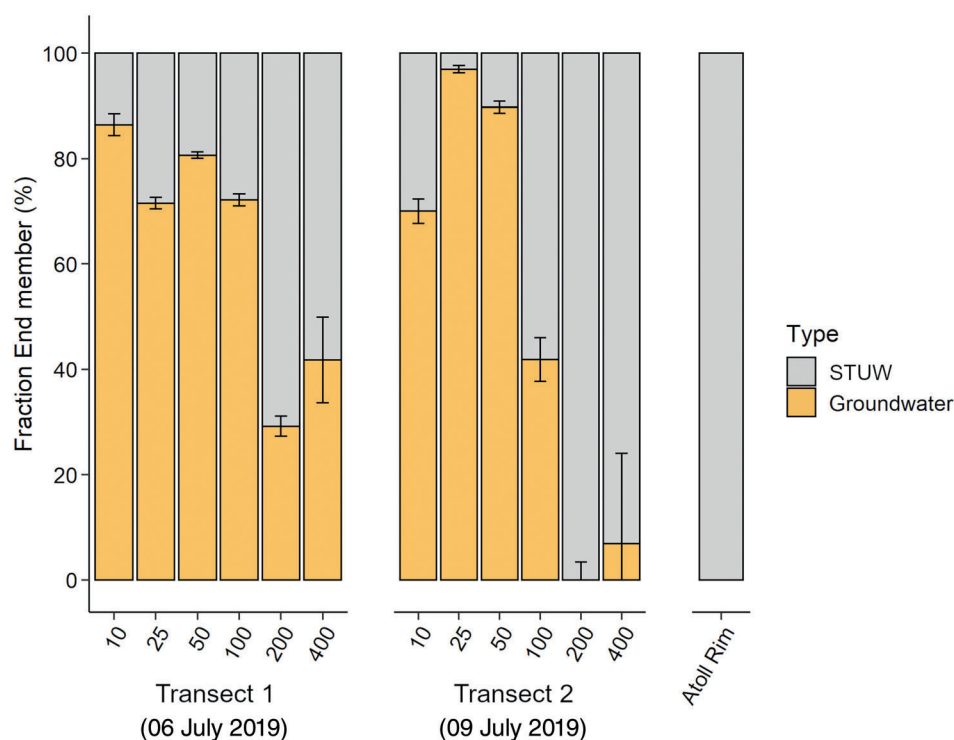
Fig. 4. The comprehensive sampling design used in this study allows us to calculate the respective contribution of the groundwater (orange bars) and ocean (Subtropical Upper Water, STUW, gray bars) isotopic end-members to the $NO_3^- + NO_2^-$ pool across the reef flat. This simple mixing was applied to the data collected along the reef flat at two occasions. The 1st transect (06 July) was collected at high tide, while the 2nd transect (09 July) was sampled shortly after a low tide (*see* Fig. 2a).

water column offshore of Surprise Island (Supporting Information Text S2). This information is relevant here to understand the processes at play within the groundwater, and these data will be presented and discussed accordingly below.
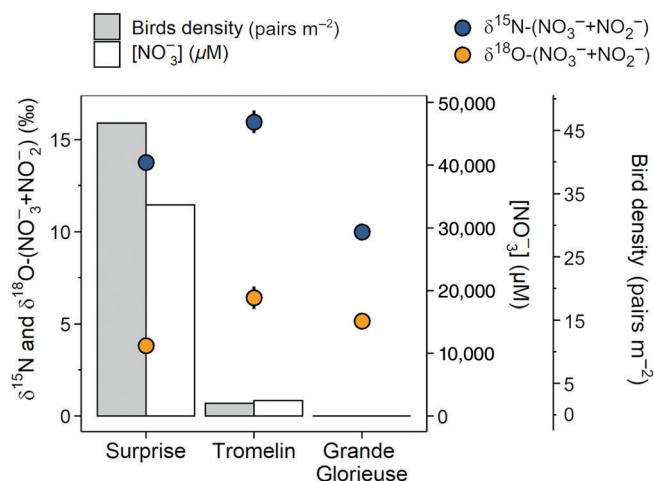

Fig. 5. Seabird density on the nesting tropical islands studied (gray bars, in breeding pair m^{-2}) appears to control mainly the NO_3^- concentration in the groundwater (white bars), with high bird densities linked to high NO_3^- concentrations. The N and O isotopes of $(NO_3^- + NO_2^-)$ (blue and orange circles respectively) are likely driven by other factors (*see* the text).

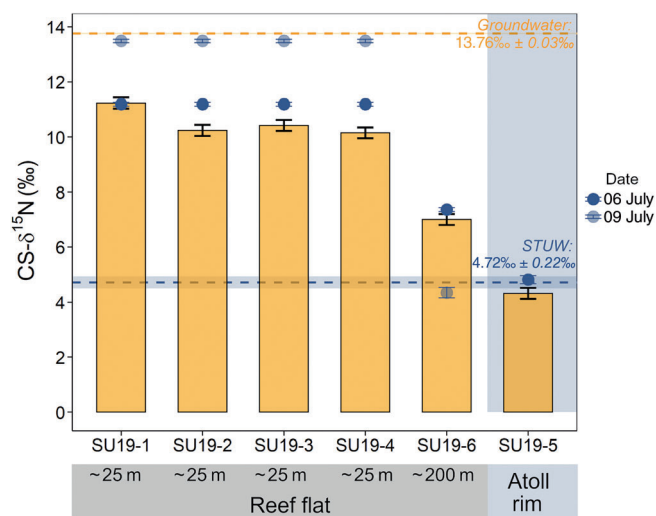**Fig. 6.** Comparison of coral skeleton $\delta^{15}N$ (CS-$\delta^{15}N$—orange bars, SD ± 0.2 for the analytical error) with the $\delta^{15}N$ of $(NO_3^- + NO_2^-)$ of the surrounding water mass (blue circles) on 06 July (high tide, darker marker) and 09 July (low tide, lighter marker). Corals SU19-1 to SU19-4 were collected 25 m and SU19-6 200 m from shore on the reef flat. Coral SU19-5 was collected at the atoll rim site (Fig. 1c,d). End-members are represented as dashed lines. As such CS-$\delta^{15}N$ records have the potential to unveil the dynamic of the various N-sources present on the reef like groundwater (orange dashed line) and oceanic water identified as STUW (blue dashed line) over time, using coral cores.

The water column was stratified offshore from the island, with a MLD estimated at 79.5 m (Fig. 3). Surface offshore NO_3^- concentration was similarly low as the values found at the edge of the reef flat ($0.03 \pm 0.01\,\mu M$). NO_3^- concentration increased consistently with depth, reaching a value of $14.90 \pm 0.10\,\mu M$ at 500 m. $\delta^{15}N - (NO_3^- + NO_2^-)$ reached a subsurface minimum of $4.72‰ \pm 0.22‰$ below the MLD at 100 m depth, and ranged between $6.79‰ \pm 0.03‰$ and $6.98‰ \pm 0.05‰$ between 200 and 500 m depth. The subsurface minimum was absent from the isotopic signature of samples without NO_2^-.

$\delta^{18}O\text{-}H_2O$ values were relatively constant throughout the water column, ranging between $-0.3‰$ and $0.1‰$. The observed increase in $\delta^{18}O\text{-}H_2O$ (from $-0.3‰$ to $0.1‰$) occurred between 400 and 300 m depth, and was accompanied by a decrease in $\delta^{18}O - (NO_3^- + NO_2^-)$ from $3.48‰$ to $2.55‰ \pm 0.20‰$ across this depth range (Fig. 3e). The deepest open ocean $\delta^{18}O - (NO_3^- + NO_2^-)$ measurement (500 m) was $3.40‰ \pm 0.24‰$.

Along the reef flat transect, surface water NO_3^- concentrations changed from $5.65 \pm 0.54\,\mu M$ at the coast to less than $0.20\,\mu M$ at 400 m from shore (Fig. 2b). NH_4^+ and urea represented a much smaller portion of available dissolved N, ranging from 0.55 to 0.06 μM (NH_4^+) and 0.36 to 0.16 μM (urea) on the reef flat (Supporting Information Table S2). Interestingly, different trends in the NO_3^- concentration were observed along the transect, depending on the sampling date and the tide phase. The first transect, on 06 July 2019, was sampled when the water column height was at a local maximum (Fig. 2a), and showed a decrease in NO_3^- concentrations from $4.82 \pm 0.05\,\mu M$ at 10 m to $0.13 \pm 0.01\,\mu M$ 400 m away from shore, with a local NO_3^- minimum occurring at 25 m ($2.05 \pm 0.01\,\mu M$; Fig. 2b). The second transect was sampled on 09 July 2019, shortly after the low tide minimum (Fig. 2a) and showed an increase in NO_3^- concentration from $2.04 \pm 0.49\,\mu M$ at 10 m to $5.65 \pm 0.54\,\mu M$ 25 m away from shore, followed by a decrease to $0.27 \pm 0.01\,\mu M$ at the most distal location (Fig. 2b).

Groundwater samples had NO_3^- concentrations more than 5000 times higher than was observed along the reef-flat or deep ocean NO_3^- ($27,000–37,300\,\mu M$, Fig. 2b). Groundwater $\delta^{15}N - NO_3^-$ values ($13.73‰ \pm 0.05‰$, Fig. 2c; Supporting Information Table S2) and $\delta^{18}O - NO_3^-$ values ($3.97‰ \pm 0.30‰$, Fig. 2d; Supporting Information Table S2) were similar to those observed at near-shore stations on the reef flat transect, while $\delta^{18}O\text{-}H_2O$ was much lower, around $-3.3‰ \pm 0.1‰$ (Fig. 2e; Supporting Information Table S2). Unlike reef flat or open ocean waters, the brackish groundwater (of salinity 14) also had a high NH_4^+ and urea content (Supporting Information Table S2).

N sources mixing on the reef flat

Several water masses were identified offshore of Surprise Island (Supporting Information Fig. S1; Text S1; Table S3). A comparison of $\delta^{15}N - (NO_3^- + NO_2^-)$ and $(NO_3^- + NO_2^-)$ concentrations showed mixing between two major water masses on the reef: (1) the groundwater (100% seabird-derived $NO_3^- + NO_2^-$), after dilution with seawater, and (2) the Subtropical Upper Water (STUW; Supporting Information Fig. S2). Assuming that these are the dominant water masses at play on the reef flat, we calculated the proportion of each of the two sources across the reef flat, for the two time points sampled (06 July and 09 July, Fig. 2a). Our data suggest that groundwater $(NO_3^- + NO_2^-)$ explained 70–97% of the $NO_3^- + NO_2^-$ pool on the first 50 m of the reef flat and represented up to 72% of the $NO_3^- + NO_2^-$ pool up to 100 m from the shore on both sampled dates (Fig. 4; Supporting Information Table S2).

Seabird-derived N and seabird density

We compared Surprise Island groundwater samples to those from Tromelin, another bird-nesting island that hosts more than 2000 seabird breeding pairs (Le Corre et al. 2015), and to Grande Glorieuse, a seabird-free island (Fig. 5) in the Indian Ocean. The $\delta^{18}O - NO_3^-$ and $\delta^{18}O\text{-}H_2O$ were similar at each of the three sites, as were the $\delta^{18}O - NO_3^-$ of groundwater and oceanic waters surrounding the island (Supporting Information Table S2). Groundwater isotope measurements showed that seabird-nesting sites had high $\delta^{15}N - NO_3^-$ values, ranging from 13.73‰ to 16.40‰, while the bird-free island had lower values ($10.23‰ \pm 0.01‰$, Fig. 5). NO_3^- concentration was 14 times higher in the groundwater at Surprise, where the seabird density was almost 20 times greater than at Tromelin, and more than 4000 times greater than the groundwater at Grande Glorieuse (Fig. 5).

CS-$\delta^{15}N$ measurements

The coral cores collected from the reef flat of Surprise Island had high CS-$\delta^{15}N$ values that decreased from $10.5‰ \pm 0.5‰$ to 7.0‰ between 25 and 200 m distance from the island (Fig. 6). These values were similar to or differed by 1‰ from the $\delta^{15}N\text{-}(NO_3^- + NO_2^-)$ of seawater at these sites. At the atoll rim site (SU 19-5), the CS-$\delta^{15}N$ value was 4.3‰, a value similar to the $\delta^{15}N - (NO_3^- + NO_2^-)$ of the STUW (Fig. 6). CS-$\delta^{15}N$ values were also relatively close to ambient $\delta^{15}N\text{-PN}$, which ranged between 9.2‰ and 5.8‰ (Fig. 7).

Discussion

Properties of the Coral Sea's thermocline water masses

Constraining the isotopic fingerprint ($\delta^{15}N$, $\delta^{18}O$) of the NO_3^- of the various water masses found in the upper 500 m of the Coral Sea (i.e., the thermocline) is critical in order to characterize the origin of the oceanic NO_3^- supply to coral reef ecosystems in the region. $\delta^{15}N$- and $\delta^{18}O - NO_3^-$ values in this region are scarce, especially for the upper 100 m of the water column, where the NO_3^- concentration is typically $<0.5\,\mu M$ (Rafter and Sigman 2016; Fripiat et al. 2021). Here, we provide the first measurements of dual isotopes NO_3^- ratio in the various water masses of the thermocline of the eastern Coral Sea.
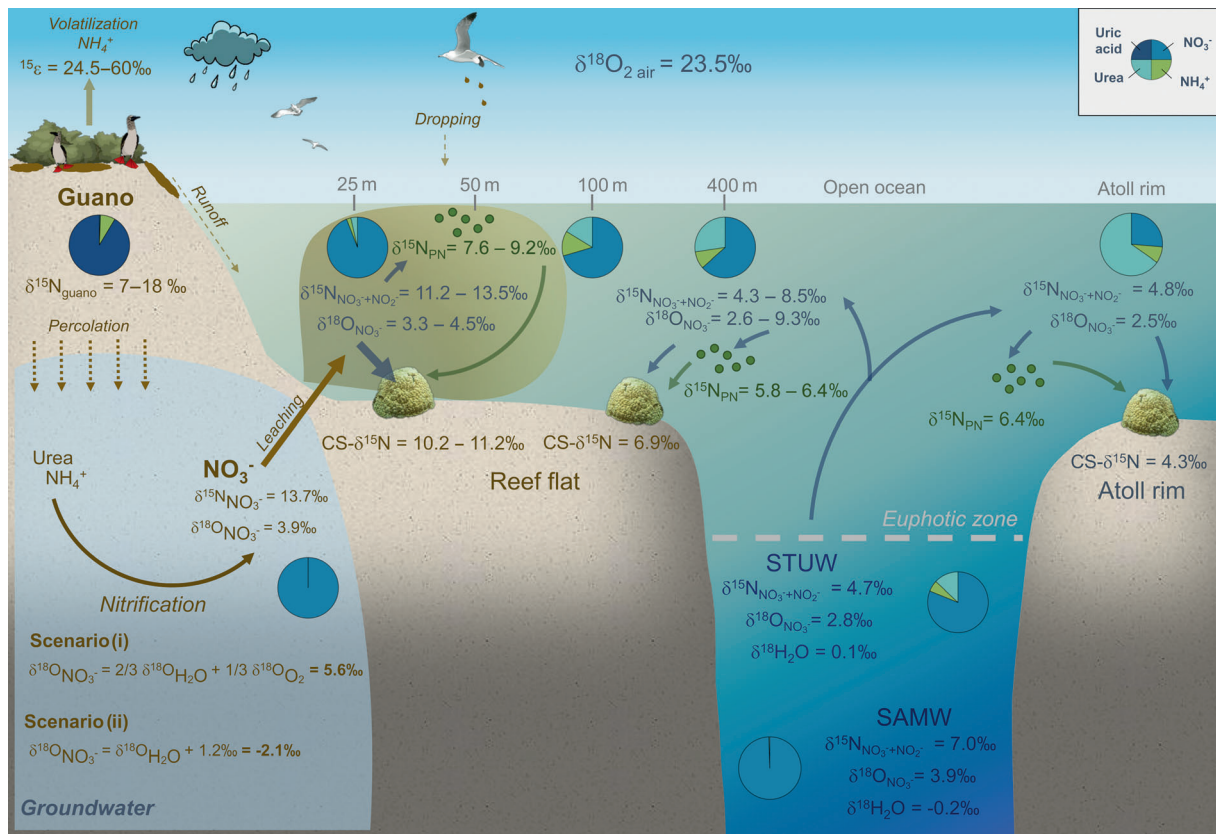
Fig. 7. Summary diagram of the transfer and the transformation of seabird-derived N across the land-sea continuum of a tropical nesting island. Seabird-derived N is indicated by brown arrows. Green arrows illustrate the transfer from PN to corals, while blue arrows account for NO_3^- assimilation. As discussed in the text, seabird-derived N mostly percolates in the groundwater lens where it is transformed into NO_3^- through nitrification. This process generates $\delta^{15}N - (NO_3^- + NO_2^-)$ with an isotopic composition similar to its N-source (here, guano), and a $\delta^{18}O - NO_3^-$ between $-2.1‰$ and $5.6‰$ depending on the scenario considered. Leaching on the reef-flat induces inputs of enriched $\delta^{15}N - (NO_3^- + NO_2^-)$ up to 100 m from shore and seems to be consumed by corals, while lighter $\delta^{15}N$-PN is less likely to be the main N-source to corals there. While $(NO_3^- + NO_2^-)$ is relevant for isotope budgeting, $\delta^{18}O - (NO_3^- + NO_2^-)$ values may be artificially low because of the low $\delta^{18}O$ of measured NO_2^- (Casciotti et al. 2007). Therefore, only $\delta^{18}O - NO_3^-$ alone are presented here. The pie charts present the nutrient content at each site averaged between our two sampling dates (*see* Supporting Information Table S2). Nutrient content of guano was estimated from Staunton Smith and Johnson (1995).

The main oceanic NO_3^- pool, by concentration, is the Subantarctic Mode Water (SAMW, S5), identified at 500 m depth, with a $\delta^{15}N$-NO_3^- of $7.19‰ \pm 0.04‰$ and a concentration of $14.90 \pm 0.10 \, \mu M$ (Supporting Information Table S3). Above the SAMW lies the warmer and more saline waters of the STUW (Supporting Information Fig. S1). The STUW, at around 100 m depth, is characterized by a salinity maximum, a low NO_3^- concentration, and a $\delta^{15}N$-$(NO_3^- + NO_2^-)$ minimum ($4.72‰ \pm 0.22‰$, Fig. 3d). These depth profile data suggest that the oceanic $(NO_3^- + NO_2^-)$ pool undergoes several processes in the surface layer (i.e., < 100 m) (discussed in Supporting Information Text S2) and that the water at 100 m depth supplies $(NO_3^- + NO_2^-)$ to the euphotic zone. The additional similarity between the $\delta^{15}N - (NO_3^- + NO_2^-)$ of this water mass and the one measured at Surprise Island, 200 and 400 m from shore (i.e., at the end of the reef flat, Fig. 2c), allows us to interpret the STUW as the main source of oceanic $(NO_3^- + NO_2^-)$ supply to the reef, better than the reef samples themselves, which

may have been influenced by NO_3^- assimilation, nitrification, groundwater N inputs, and other processes in a complex sequence. Thus, the $\delta^{15}N$ of the oceanic NO_3^- end-member is well constrained, and its properties allow tracing the STUW within the reef system.

Coral islands' groundwater is a biological reactor for N species

The present study suggests that the NO_3^- in the groundwater present in Surprise Island's framework could be an important source of N to the surrounding reef. In fact, the NO_3^- concentration observed in Surprise Island's groundwater ($27,000-37,300 \, \mu M$, Fig. 2b) is three orders of magnitude greater than the one observed in the STUW at the study site. It is more than 10 times higher than the values previously reported for the groundwater of other remote and/or seabird-nesting atolls (Tait et al. 2014; O'Reilly et al. 2015; McMahon and Santos 2017), although the link between seabird density and the

properties of the groundwater for a given tropical island may yield insight into the role of seabird population in shaping the size of the NO_3^- reservoir of the water table (more in depth discussion about this topic can be found in the Supporting Information Text S3). It is also significantly higher than concentrations found in urban areas and NO_3^--contaminated groundwater (ranging between 0.07 and 13 mM; Wassenaar 1995; Montiel et al. 2019; Sims et al. 2020), stressing the relevance of Surprise Island's groundwater as a major reservoir of NO_3^-. The groundwater at Surprise Island is also characterized by elevated $\delta^{15}N - \left(NO_3^- - NO_2^-\right)$ (13.76‰ $\pm$ 0.03‰; Fig. 2c). These high values are similar in magnitude to existing observations of $\delta^{15}N - \left(NO_3^- - NO_2^-\right)$ measured in groundwater influenced by poultry manure, which ranged between 8‰ and 16‰ (Wassenaar 1995), suggesting that groundwater at Surprise Island is influenced by similar processes.

At first glance, the high NO_3^- concentration in the groundwater of Surprise Island seems at odds with the relatively low NO_3^--content of the seabird droppings; indeed, seabird feces typically contain 8–21% N by mass, which is made up of uric acid ($\sim 80\%$), NH_4^+ ($\sim 7\%$) and NO_3^- ($\sim 0.5\%$) (Staunton Smith and Johnson 1995). In addition, although dissolution experiments show that less than 0.02% of the guano N is released in solution in the form of NO_3^- (Loder et al. 1996), NO_3^- represents 99% of the groundwater dissolved N-pool at Surprise Atoll (Supporting Information Table S2; Fig. 7). This strongly suggests that chemical transformations are taking place during the transfer of seabird-derived N into the groundwater.

The elevated groundwater NO_3^- concentrations, along with our dual isotope measurements, point to the coupled ammonification/nitrification of reduced seabird-derived N species into NO_3^- in the groundwater to explain the observed properties of the groundwater. Both uric acid and NH_4^+ contained in seabird feces are subject to prompt biotic (i.e., bacterial) and abiotic transformations (i.e., volatilization) in aerobic settings; NH_4^+ is readily available for nitrification, and uric acid becomes rapidly available once remineralized into NH_4^+ during ammonification processes (Wright 1995; Otero et al. 2018). The moderate $\delta^{15}N$ elevation observed in the NO_3^- compared to the broad range identified for guano $\delta^{15}N$ (ranging from 7‰ to 18‰ between "relatively fresh" and "aged" guano; Lorrain et al. 2017; Thibault et al. 2022), could simply arise from the mixture of guano representing each extremes. For example, assuming arbitrarily that 50% of fresh and 50% of dried guano leach into the groundwater lens, with no fractionation during nitrification (nitrification of the entirety of NH_4^+ produced), we would expect a $\delta^{15}N - NO_3^-$ of $\sim 12.5\%$, a value relatively close to the $\delta^{15}N - NO_3^-$ we measured (13.73‰ $\pm$ 0.05‰, Fig. 2c). Although the influence of guano ageing on the N isotope fractionation is beyond the scope of this study, we discuss some possible mechanisms in the Supporting Information Text S4.

Nitrification in groundwater imprints the $\delta^{18}O$ values of both O_2 and H_2O, although the extent to which this alters $\delta^{18}O - NO_3^-$ is debated. Biochemical studies suggest that during nitrification, one atom of the NO_3^- produced is supplied by molecular O_2 (which has a $\delta^{18}O$ of $\sim 23.5\%$; Barkan and Luz 2005) and two atoms by ambient H_2O (Andersson and Hooper 1983; Kumar et al. 1983). However, in some systems like the deep ocean, $\delta^{18}O$ measurements of NO_3^- suggest a much smaller contribution from molecular O_2 ($\sim 1/6$; Casciotti et al. 2002). Indeed, oceanic NO_3^- isotope measurements appear to call for an even smaller influence of O_2 on $\delta^{18}O - NO_3^-$ (Sigman et al. 2009), consistent with subsequent studies reporting $\delta^{18}O$ values of newly nitrified NO_3^- being 1.1–1.2‰ higher than that of ambient water (Granger et al. 2013; Marconi et al. 2019). The $\delta^{18}O$ of H_2O in the groundwater of our study sites (Tromelin, Grande Glorieuse and Surprise) ranged between -2.8% and -4.3% and averaged $-3.3\% \pm 0.2\%$ at Surprise Island (Supporting Information Table S2), in agreement with the range of $\delta^{18}O$ values of precipitation at this latitude (from -2% to -6%, Feng et al. 2009). We estimate the expected $\delta^{18}O$ of newly nitrified NO_3^- in Surprise Island groundwater considering the following end-member scenarios for O atom incorporation: (i) one out of three O atoms come from O_2 and (ii) all of the O atoms derive from ambient water. For (i), we calculate a theoretical $\delta^{18}O$ of nitrified NO_3^- in groundwater of 5.6‰, a value less than 2‰ higher than the one observed at Surprise Island (Supporting Information Table S2). For (ii), we calculate a $\delta^{18}O$ of -2.1%, $\sim 6\%$ lower than that of the groundwater NO_3^-. While we cannot firmly validate one scenario over the other, these results give a range of possible $\delta^{18}O$ of newly nitrified NO_3^- which encompasses our measured value (3.97‰ $\pm$ 0.30‰; Fig. 5).

The significantly lower $\delta^{18}O$ estimated with (ii) relative to the actual data could suggest that denitrification might be at play at our study site. But given the strong N and O isotopic discriminations associated with denitrification (Granger et al. 2008; Kritee et al. 2012), the similarity of the $\delta^{18}O - NO_3^-$ and $\delta^{18}O\text{-}H_2O$ values found at Surprise on the reef and oceanic station, Tromelin and Grande Glorieuse islands (Fig. 5; Supporting Information Table S2) argues for at most a modest role for denitrification in elevating the $\delta^{15}N$- and $\delta^{18}O - NO_3^-$ of groundwater. In addition, the very thin soil layer found on the island (MT, AL, ND, pers. obs. 2019) and the coarse, well-aerated coral debris making the bulk of the island mass (i.e., mm-size sand grain; Andréfouët et al. 2009) works against the development of anoxia required for denitrification to take place. Thus, most of the $\delta^{15}N$ elevation that we observe in groundwater NO_3^- must derive from the high $\delta^{15}N$ of the N deriving from guano (likely uric acid and NH_4^+), which suggests that nitrification plays a significant role in transforming seabird-derived N inputs within groundwater systems as observed for poultry-derived N (Wassenaar 1995). The oxidation of seabird-derived N is most likely complete, as

no NO_2^-, the intermediate between NH_4^+ and NO_3^- during nitrification, was detected in this reservoir.

Groundwater supply to the reef flat

With biological consumption as a dominant process in the euphotic zone, we would expect to see an increase in $\delta^{15}N - (NO_3^- + NO_2^-)$ with decreasing NO_3^- concentration (Swart et al. 2014; Erler et al. 2015) along the reef flat. Instead, the positive nonlinear trend between NO_3^- concentrations and $\delta^{15}N - (NO_3^- + NO_2^-)$ along transect (Supporting Information Fig. S2) indicates that mixing between the groundwater and the STUW primarily explains the distribution of $(NO_3^- + NO_2^-)$ here (Wankel et al. 2007; Sims et al. 2020). Beyond 100 m from shore, the $\delta^{15}N$-$(NO_3^- + NO_2^-)$ values resemble those of the oceanic end-member (i.e., STUW), indicating that the dilution of the groundwater over the reef flat was completed at $\sim$100 m at the time of sampling (Supporting Information Fig. S2).

Although groundwater NO_3^- seems to have a significant influence on the adjacent reef, the pathway by which it is transferred to the reef flat remains poorly constrained. Strong salinity drops recorded by the data loggers deployed along the reef flat evidenced the leaching of brackish (salinity 14), high NO_3^-, and high $\delta^{15}N$ groundwater (Fig. 2a), depending on the tidal regime. These salinity anomalies were particularly pronounced at 25 m, where the peak in NO_3^- concentration and similarities between seawater and groundwater $\delta^{15}N$-$(NO_3^- + NO_2^-)$ at low tide (09 July) confirm the influence of groundwater at that site. The 25-m site is located at the edge of an extensive beachrock outcrop protruding from the beach, similar to the beachrock layer found above the water table during the dig of the borehole, suggesting the presence of an interface between groundwater and the ocean at that site.

These observations imply that neither runoff nor direct droppings play a significant role in seabird-derived N transport across the land–sea continuum. Instead, our data suggest that the main pathway from land to sea at Surprise Atoll is the transfer of N from deposited feces to the groundwater, where it is bacterially oxidized into NO_3^- and subsequently leached to the reef through the porous carbonate atoll substrate 25 m from shore, most likely via tidal pumping. The groundwater lens acts as a powerful bioreactor that transforms most of the seabird-derived N to NO_3^- via nitrification, making this N form dominant on the reef flat. Questions regarding the rates of transport of groundwater NO_3^- onto the reef, the groundwater residence time, the influence of rainfall on the groundwater discharge, and groundwater N-cycling along the reef flat are beyond the scope of this paper, but with further attention could clarify the questions raised in the preceding paragraphs.

Coral skeleton $\delta^{15}N$ records $\delta^{15}N - (NO_3^- + NO_2^-)$

This study, along with previous research (Lorrain et al. 2017; Thibault et al. 2022), confirms the significant influence of seabird-derived N on Surprise Island reef flat in shaping the isotopic composition of NO_3^-, macroalgae, coral tissues and coral endosymbionts alike. While this extensive dataset convincingly demonstrates seabird-N's importance in the nearshore N budget and helps trace N transfer along the land–ocean continuum, it only provides short-term snapshots ranging from minutes (NO_3^- isotopes) to weeks (macroalgae) or months (coral tissues). This limitation prevents us from identifying potential shifts in N sources or fluctuations in N supply over longer time scales in response to climate variability (i.e., El Niño Southern Oscillation, Pacific Decaldal Oscillat) or anthropogenic impacts (e.g., introduction of invasive species, guano mining). The N isotopic composition of the organic matter encapsulated in coral skeletons faithfully records the isotopic composition of the coral's N source, and it is protected from potential diagenetic alterations by the mineral matrix (Wang et al. 2014, 2016; Martínez-García et al. 2022). In fact, CS-$\delta^{15}N$ records obtained from the massive coral *Porites* have been proven to be an excellent tool for generating monthly resolved CS-$\delta^{15}N$ time-series capturing changes in N-sources and cycling over decades or centuries (Wang et al. 2018; Murray et al. 2019; Duprey et al. 2020).

Here, we tested whether *Porites* CS-$\delta^{15}N$ could also be used to reconstruct the history of seabird-N inputs by evaluating how this coral genus records the $\delta^{15}N - (NO_3^- + NO_2^-)$ gradient across the reef flat. The CS-$\delta^{15}N$ measured on the six coral cores closely tracked the $\delta^{15}N - (NO_3^- + NO_2^-)$ values found at high tide (Fig. 6). Consequently, calculation of N sources contributions to the reef flat (groundwater and STUW) calculated from the CS-$\delta^{15}N$ values yield contributions of groundwater of about 65% at 25 m, 25% at 200 m, and 0% on the atoll rim, in agreement with the $\delta^{15}N - (NO_3^- + NO_2^-)$ data (Fig. 4).

N assimilation pathways in scleractinian corals is an active field of research, and the sampling design used here was not intended to address this issue. Coral N supply relies on two main pathways: PN (by feeding) that ultimately derives its N from dissolved N (Houlbrèque and Ferrier-Pagès 2009) and dissolved N itself (i.e., NH_4^+, urea, amino acids, NO_3^-), translocated from the symbiont to the host, by transfer of N-bearing compounds (Martinez et al. 2022) or by symbiont pruning (Boschma 1925; Wiedenmann et al. 2023). On the reef flat and at the atoll rim, the relative similarity of $\delta^{15}N - (NO_3^- + NO_2^-)$, $\delta^{15}N$-PN, and CS-$\delta^{15}N$ values do not allow the stable isotopes to clarify N assimilation pathways for *Porites*. It is thus likely that both mechanisms are contributing to the coral N requirements at these sites, in varying proportions, as observed in *Pocillopora damicornis* (Thibault et al. 2022). Regardless, in all cases, the CS-$\delta^{15}N$ tracks the ambient $\delta^{15}N - (NO_3^- + NO_2^-)$ and records the high $\delta^{15}N$ signal associated with guano inputs to the reef system. As such, with a careful spatial sampling design, *Porites* CS-$\delta^{15}N$ records have the potential to disentangle changes occurring in the sources of N identified in the system (i.e., end-members) while also allowing for the reconstruction of the respective contribution of each N source at a given location over the past decades or centuries.

Conclusions

We used natural abundance stable isotopic measurements to trace the fate of seabird-derived N in a tropical seabird nesting coral island, characterizing the various transformations of N species throughout the land–sea continuum and identifying the processes that control these transformations. Our measurements demonstrated the key role of the groundwater reservoir in converting reduced seabird-N species to NO_3^-, and emphasize the significance of groundwater as major source of N. The NO_3^- from groundwater is the main supply of NO_3^- to the adjacent reef flat, in contrast to the coral reefs along the atoll rim, which receive most of their N supply from the thermocline. *Porites* CS-δ^{15}N records faithfully the contribution of the various N sources to the reef flat and could be used to assess the dynamics of seabird-derived N to the coral reef over time. Such an application would provide an invaluable tool for reconstructing the demographic history of tropical seabird population following anthropogenic disturbances (rats' introduction, overfishing, and climate change).

Data availability statement

All data associated with this manuscript (visible in Supporting Information Table S2) are available in DataVerse Repository (https://doi.org/10.7910/DVN/QSHDVR).

References

Altieri, K. E., M. G. Hastings, A. J. Peters, S. Oleynik, and D. M. Sigman. 2014. Isotopic evidence for a marine ammonium source in rainwater at Bermuda. Global Biogeochem. Cycl. **28**: 1066–1080. doi:10.1002/2014GB004809

Aminot, A., and R. Kerouel. 1982. Dosage automatique de l'urée dans l'eau de mer: une méthode très sensible à la diacétylmonoxime. Can. J. Fish. Aquat. Sci. **39**: 174–183. doi:10.1139/f82-020

Anderson, W. B., and G. A. Polis. 1998. Marine subsidies of Island communities in the Gulf of California: Evidence from stable carbon and nitrogen isotopes. Oikos **81**: 75. doi:10.2307/3546469

Anderson, W. B., and G. A. Polis. 1999. Nutrient fluxes from water to land: Seabirds affect plant nutrient status on Gulf of California islands. Oceologia **118**: 324–332.

Andersson, K. K., and A. B. Hooper. 1983. O_2 and H_2O are each the source of one O in NO_2^- produced from NH_3 by *Nitrosomonas*: ^{15}N-NMR evidence. FEBS Lett. **164**: 236–240. doi:10.1016/0014-5793(83)80292-0

Andréfouët, S., G. Cabioch, B. Flamand, and B. Pelletier. 2009. A reappraisal of the diversity of geomorphological and genetic processes of New Caledonian coral reefs: A synthesis from optical remote sensing, coring and acoustic multibeam observations. Coral Reefs **28**: 691–707. doi:10.1007/s00338-009-0503-y

Barkan, E., and B. Luz. 2005. High precision measurements of ^{17}O/^{16}O and ^{18}O/^{16}O ratios in H_2O. Rapid Commun. Mass Spectrom. **19**: 3737–3742. doi:10.1002/rcm.2250

Benkwitt, C. E., S. K. Wilson, and N. A. J. Graham. 2019. Seabird nutrient subsidies alter patterns of algal abundance and fish biomass on coral reefs following a bleaching event. Glob. Chang. Biol. **25**: 2619–2632. doi:10.1111/gcb.14643

Benkwitt, C. E., R. L. Gunn, M. Le Corre, P. Carr, and N. A. J. Graham. 2021. Rat eradication restores nutrient subsidies from seabirds across terrestrial and marine ecosystems. Curr. Biol. **31**: 2704–2711.e4. doi:10.1016/j.cub.2021.03.104

Blackall, T. D., L. J. Wilson, J. Bull, M. R. Theobald, P. J. Bacon, K. C. Hamer, S. Wanless, and M. A. Sutton. 2008. Temporal variation in atmospheric ammonia concentrations above seabird colonies. Atmos. Environ. **42**: 6942–6950. doi:10.1016/j.atmosenv.2008.04.059

Bonnet, S., and others. 2015. Contrasted geographical distribution of N_2 fixation rates and *nif* H phylotypes in the Coral and Solomon Seas (southwestern Pacific) during austral winter conditions. Global Biogeochem. Cycl. **29**: 1874–1892. doi:10.1002/2015GB005117

Boschma, H. 1925. On the feeding reactions and digestion in the coral polyp *Astrangia danæ*, with notes on its symbiosis with zoöxanthellæ. Biol. Bull. **49**: 407–439. doi:10.2307/1536652

Braman, R. S., and S. A. Hendrix. 1989. Nanogram nitrite and nitrate determination in environmental and biological materials by vanadium(III) reduction with chemiluminescence detection. Anal. Chem. **61**: 2715–2718. doi:10.1021/ac00199a007

Burkepile, D. E., and others. 2020. Nitrogen identity drives differential impacts of nutrients on coral bleaching and mortality. Ecosystems **23**: 798–811. doi:10.1007/s10021-019-00433-2

Carpenter, E. J., H. R. Harvey, B. Fry, and D. G. Capone. 1997. Biogeochemical tracers of the marine cyanobacterium *Trichodesmium*. Deep-Sea Res. I Oceanogr. Res. Pap. **44**: 27–38. doi:10.1016/S0967-0637(96)00091-X

Casciotti, K. L., D. M. Sigman, M. G. Hastings, J. K. Böhlke, and A. Hilkert. 2002. Measurement of the oxygen isotopic composition of nitrate in seawater and freshwater using the denitrifier method. Anal. Chem. **74**: 4905–4912. doi:10.1021/ac020113w

Casciotti, K. L., J. K. Böhlke, M. R. McIlvin, S. J. Mroczkowski, and J. E. Hannon. 2007. Oxygen isotopes in nitrite: Analysis, calibration, and equilibration. Anal. Chem. **79**: 2427–2436. doi:10.1021/ac061598h

DeCarlo, T. M., and others. 2020. Nutrient-supplying ocean currents modulate coral bleaching susceptibility. Sci. Adv. **6**: eabc5493. doi:10.1126/sciadv.abc5493

Dubinsky, Z., and I. Berman-Frank. 2001. Uncoupling primary production from population growth in photosynthesizing organisms in aquatic ecosystems. Aquat. Sci. **63**: 4–17. doi:10.1007/PL00001343

Duprey, N. N., M. Yasuhara, and D. M. Baker. 2016. Reefs of tomorrow: Eutrophication reduces coral biodiversity in an urbanized seascape. Glob. Chang. Biol. **22**: 3550–3565. doi: 10.1111/gcb.13432

Duprey, N. N., and others. 2020. Megacity development and the demise of coastal coral communities: Evidence from coral skeleton $\delta^{15}N$ records in the Pearl River estuary. Glob. Chang. Biol. **26**: 1338–1353. doi:10.1111/gcb.14923

Erler, D. V., X. T. Wang, D. M. Sigman, S. R. Scheffers, and B. O. Shepherd. 2015. Controls on the nitrogen isotopic composition of shallow water corals across a tropical reef flat transect. Coral Reefs **34**: 329–338. doi:10.1007/s00338-014-1215-5

Fabricius, K. E., S. Cséke, C. Humphrey, and G. De'ath. 2013. Does trophic status enhance or reduce the thermal tolerance of scleractinian corals? A review, experiment and conceptual framework. PloS One **8**: e54399. doi:10.1371/journal.pone.0054399

Feng, X., A. M. Faiia, and E. S. Posmentier. 2009. Seasonality of isotopes in precipitation: A global perspective. J. Geophys. Res. **114**: D08116. doi:10.1029/2008JD011279

Fripiat, F., and others. 2021. Nitrogen isotopic constraints on nutrient transport to the upper ocean. Nat. Geosci. **14**: 855–861. doi:10.1038/s41561-021-00836-8

Fry, B. 2006. Stable isotope ecology. Springer.

Graham, N. A. J., S. K. Wilson, P. Carr, A. S. Hoey, S. Jennings, and M. A. MacNeil. 2018. Seabirds enhance coral reef productivity and functioning in the absence of invasive rats. Nature **559**: 250–253. doi:10.1038/s41586-018-0202-3

Granger, J., D. M. Sigman, J. A. Needoba, and P. J. Harrison. 2004. Coupled nitrogen and oxygen isotope fractionation of nitrate during assimilation by cultures of marine phytoplankton. Limnol. Oceanogr. **49**: 1763–1773. doi:10.4319/lo.2004.49.5.1763

Granger, J., D. M. Sigman, M. F. Lehmann, and P. D. Tortell. 2008. Nitrogen and oxygen isotope fractionation during dissimilatory nitrate reduction by denitrifying bacteria. Limnol. Oceanogr. **53**: 2533–2545. doi:10.4319/lo.2008.53.6.2533

Granger, J., and D. M. Sigman. 2009. Removal of nitrite with sulfamic acid for nitrate N and O isotope analysis with the denitrifier method. Rapid Commun. Mass Spectrom. **23**: 3753–3762. doi:10.1002/rcm.4307

Granger, J., M. G. Prokopenko, C. W. Mordy, and D. M. Sigman. 2013. The proportion of remineralized nitrate on the ice-covered eastern Bering Sea shelf evidenced from the oxygen isotope ratio of nitrate. Global Biogeochem. Cycl. **27**: 962–971. doi:10.1002/gbc.20075

Holmes, R. M., A. Aminot, R. Kérouel, B. A. Hooker, and B. J. Peterson. 1999. A simple and precise method for measuring ammonium in marine and freshwater ecosystems. Can. J. Fish. Aquat. Sci. **56**: 1801–1808.

Houlbrèque, F., and C. Ferrier-Pagès. 2009. Heterotrophy in tropical Scleractinian corals. Biol. Rev. **84**: 1–17. doi:10.1111/j.1469-185X.2008.00058.x

Houlton, B. Z., D. M. Sigman, and L. O. Hedin. 2006. Isotopic evidence for large gaseous nitrogen losses from tropical rainforests. Proc. Natl. Acad. Sci. USA **103**: 8745–8750. doi:10.1073/pnas.0510185103

Kemeny, P. C., M. A. Weigand, R. Zhang, B. R. Carter, K. L. Karsh, S. E. Fawcett, and D. M. Sigman. 2016. Enzyme-level interconversion of nitrate and nitrite in the fall mixed layer of the Antarctic Ocean. Global Biogeochem. Cycl. **30**: 1069–1085. doi:10.1002/2015GB005350

Kessler, W. S., and S. Cravatte. 2013. Mean circulation of the Coral Sea. J. Geophys. Res. Oceans **118**: 6385–6410. doi:10.1002/2013JC009117

Kritee, K., D. M. Sigman, J. Granger, B. B. Ward, A. Jayakumar, and C. Deutsch. 2012. Reduced isotope fractionation by denitrification under conditions relevant to the ocean. Geochim. Cosmochim. Acta **92**: 243–259. doi:10.1016/j.gca.2012.05.020

Kumar, S., D. J. D. Nicholas, and E. H. Williams. 1983. Definitive ^{15}N NMR evidence that water serves as a source of "O" during nitrite oxidation by *Nitrobacter agilis*. FEBS Lett. **152**: 71–74. doi:10.1016/0014-5793(83)80484-0

Le Corre, M., D. K. Danckwerts, D. Ringler, M. Bastien, S. Orlowski, C. Morey Rubio, D. Pinaud, and T. Micol (2015). Seabird recovery and vegetation dynamics after Norway rat eradication at Tromelin Island, western Indian Ocean. Biol. Conserv. **185**: 85–94. doi:10.1016/j.biocon.2014.12.015

Loder, T. C., B. Ganning, and J. A. Love. 1996. Ammonia nitrogen dynamics in coastal rockpools affected by gull guano. J. Exp. Mar. Biol. Ecol. **196**: 113–129. doi:10.1016/0022-0981(95)00126-3

Lorrain, A., and others. 2017. Seabirds supply nitrogen to reef-building corals on remote Pacific islets. Sci. Rep. **7**: 3721. doi:10.1038/s41598-017-03781-y

Marconi, D., M. A. Weigand, and D. M. Sigman. 2019. Nitrate isotopic gradients in the North Atlantic Ocean and the nitrogen isotopic composition of sinking organic matter. Deep-Sea Res. I Oceanogr. Res. Pap. **145**: 109–124. doi:10.1016/j.dsr.2019.01.010

Martinez, S., R. Grover, D. M. Baker, and C. Ferrier-Pagès. 2022. Symbiodiniaceae are the first site of heterotrophic nitrogen assimilation in reef-building corals. mBio **13**: e01601–e01622. doi:10.1128/mbio.01601-22

Martínez-García, A., and others. 2022. Laboratory assessment of the impact of chemical oxidation, mineral dissolution, and heating on the nitrogen isotopic composition of fossil-bound organic matter. Geochem. Geophys. Geosyst. **23**: e2022GC010396. doi:10.1029/2022GC010396

McDougall, T. J. 1987. Neutral surfaces. J. Phys. Oceanogr. **17**: 1950–1964. doi:10.1175/1520-0485(1987)017<1950:NS>2.0.CO;2

McIlvin, M. R., and K. L. Casciotti. 2011. Technical updates to the bacterial method for nitrate isotopic analyses. Anal. Chem. **83**: 1850–1856. doi:10.1021/ac1028984

McMahon, A., and I. R. Santos. 2017. Nitrogen enrichment and speciation in a coral reef lagoon driven by groundwater

inputs of bird guano. J. Geophys. Res. Oceans **122**: 7218–7236. doi:10.1002/2017JC012929

Montiel, D., and others. 2019. Natural groundwater nutrient fluxes exceed anthropogenic inputs in an ecologically impacted estuary: Lessons learned from Mobile Bay, Alabama. Biogeochemistry **145**: 1–33. doi:10.1007/s10533-019-00587-0

Moretti, S., N. N. Duprey, A. D. Foreman, A. Arns, S. Brömme, J. Jung, X. E. Ai, A. Auderset, A. L. Bieler, C. Eck, J. Farmer, B. Hinnenberg, M. Lacerra, J. Leichliter, T. Lüdecke, S. Oleynik, F. Rubach, M. Schmitt, M. Vink, … A. Martínez-García. 2023. Analytical improvements and assessment of long-term performance of the oxidation–denitrifier method. Rapid Commun. Mass Spectrom. **38**(1). Portico. doi:10.1002/rcm.9650

Murray, J., N. G. Prouty, S. Peek, and A. Paytan. 2019. Coral skeleton $\delta^{15}N$ as a tracer of historic nutrient loading to a coral reef in Maui, Hawaii. Sci. Rep. **9**: 5579. doi:10.1038/s41598-019-42013-3

Muscatine, L., C. Goiran, L. Land, J. Jaubert, J.-P. Cuif, and D. Allemand. 2005. Stable isotopes ($\delta^{13}C$ and $\delta^{15}N$) of organic matrix from coral skeleton. Proc. Natl. Acad. Sci. USA **102**: 1525–1530. doi:10.1073/pnas.0408921102

O'Reilly, C., I. R. Santos, T. Cyronak, A. McMahon, and D. T. Maher. 2015. Nitrous oxide and methane dynamics in a coral reef lagoon driven by pore water exchange: Insights from automated high-frequency observations. Geophys. Res. Lett. **42**: 2885–2892. doi:10.1002/2015GL063126

Otero, X. L., S. De La Peña-Lastra, A. Pérez-Alberti, T. O. Ferreira, and M. A. Huerta-Diaz. 2018. Seabird colonies as important global drivers in the nitrogen and phosphorus cycles. Nat. Commun. **9**: 246. doi:10.1038/s41467-017-02446-8

Philippe-Lesaffre, M., and others. 2023. Recovery of insular seabird populations years after rodent eradication. Conserv. Biol. **37**: e14042. doi:10.1111/cobi.14042

Polis, G. A., W. B. Anderson, and R. D. Holt. 1997. Toward an integration of landscape and food web ecology: The dynamics of spatially subsidized food webs. Annu. Rev. Ecol. Syst. **28**: 289–316. doi:10.1146/annurev.ecolsys.28.1.289

Rafter, P. A., and D. M. Sigman. 2016. Spatial distribution and temporal variation of nitrate nitrogen and oxygen isotopes in the upper equatorial Pacific Ocean: Equatorial Pacific nitrate N and O isotopes. Limnol. Oceanogr. **61**: 14–31. doi:10.1002/lno.10152

Russell, J. C., and M. L. Le Corre. 2009. Introduced mammal impact on seabirds in the iles eparses, Western Indian Ocean. Mar. Ornithol. **37**: 121–129.

Savage, C. 2019. Seabird nutrients are assimilated by corals and enhance coral growth rates. Sci. Rep. **9**: 4284. doi:10.1038/s41598-019-41030-6

Sigman, D. M., K. L. Casciotti, M. Andreani, C. Barford, M. Galanter, and J. K. Böhlke. 2001. A bacterial method for the nitrogen isotopic analysis of nitrate in seawater and freshwater. Anal. Chem. **73**: 4145–4153. doi:10.1021/ac010088e

Sigman, D. M., J. Granger, P. J. DiFiore, M. M. Lehmann, R. Ho, G. Cane, and A. Van Geen. 2005. Coupled nitrogen and oxygen isotope measurements of nitrate along the eastern North Pacific margin. Global Biogeochem. Cycles **19**. doi:10.1029/2005GB002458

Sigman, D. M., and others. 2009. The dual isotopes of deep nitrate as a constraint on the cycle and budget of oceanic fixed nitrogen. Deep-Sea Res. I Oceanogr. Res. Pap. **56**: 1419–1439. doi:10.1016/j.dsr.2009.04.007

Sims, Z. C., A. L. Cohen, V. H. Luu, X. T. Wang, and D. M. Sigman. 2020. Uptake of groundwater nitrogen by a nearshore coral reef community on Bermuda. Coral Reefs **39**: 215–228. doi:10.1007/s00338-019-01879-5

Staunton Smith, J., and C. Johnson. 1995. Nutrient inputs from seabirds and humans on a populated coral cay. Mar. Ecol. Prog. Ser. **124**: 189–200. doi:10.3354/meps124189

Swart, P. K., S. Evans, T. Capo, and M. A. Altabet. 2014. The fractionation of nitrogen and oxygen isotopes in macroalgae during the assimilation of nitrate. Biogeosciences **11**: 6147–6157. doi:10.5194/bg-11-6147-2014

Tait, D. R., D. V. Erler, I. R. Santos, T. J. Cyronak, U. Morgenstern, and B. D. Eyre. 2014. The influence of groundwater inputs and age on nutrient dynamics in a coral reef lagoon. Mar. Chem. **166**: 36–47. doi:10.1016/j.marchem.2014.08.004

Thibault, M., and others. 2022. Seabird-derived nutrients supply modulates the trophic strategies of mixotrophic corals. Front. Mar. Sci. **8**: 790408. doi:10.3389/fmars.2021.790408

Wang, X. T., and others. 2014. Isotopic composition of carbonate-bound organic nitrogen in deep-sea scleractinian corals: A new window into past biogeochemical change. Earth Planet. Sci. Lett. **400**: 243–250. doi:10.1016/j.epsl.2014.05.048

Wang, X. T., D. M. Sigman, A. L. Cohen, D. J. Sinclair, R. M. Sherrell, M. A. Weigand, D. V. Erler, and H. Ren. 2015. Isotopic composition of skeleton-bound organic nitrogen in reef-building symbiotic corals: A new method and proxy evaluation at Bermuda. Geochim. Cosmochim. Acta **148**: 179–190. doi:10.1016/j.gca.2014.09.017

Wang, X. T., and others. 2016. Influence of open ocean nitrogen supply on the skeletal $\delta^{15}N$ of modern shallow-water scleractinian corals. Earth Planet. Sci. Lett. **441**: 125–132. doi:10.1016/j.epsl.2016.02.032

Wang, X. T., A. L. Cohen, V. Luu, H. Ren, Z. Su, G. H. Haug, and D. M. Sigman. 2018. Natural forcing of the North Atlantic nitrogen cycle in the Anthropocene. Proc. Natl. Acad. Sci. USA **115**: 10606–10611. doi:10.1073/pnas.1801049115

Wankel, S. D., C. Kendall, J. T. Pennington, F. P. Chavez, and A. Paytan. 2007. Nitrification in the euphotic zone as evidenced by nitrate dual isotopic composition: Observations from Monterey Bay, California. Global Biogeochem. Cycl. **21**. doi:10.1029/2006GB002723

Wantiez, L., P. Frolla, and D. Goroparawa. 2022. Communautés biologiques et habitats coralliens des atolls

d'Entrecasteaux—État des lieux 2021—Maintien de l'intégrité. Onservatoire d'Espaces Naturels de Nouvelle—Calédonie, Université de la Nouvelle-Calédonie.

Wassenaar, L. I. 1995. Evaluation of the origin and fate of nitrate in the Abbotsford aquifer using the isotopes of ^{15}N and ^{18}O in NO_3^-. Appl. Geochem. **10**: 391–405. doi:10.1016/0883-2927(95)00013-A

Weigand, M. A., J. Foriel, B. Barnett, S. Oleynik, and D. M. Sigman. 2016. Updates to instrumentation and protocols for isotopic analysis of nitrate by the denitrifier method. Rapid Commun. Mass Spectrom. **30**: 1365–1383. doi:10.1002/rcm.7570

Wiedenmann, J., C. D'Angelo, E. G. Smith, A. N. Hunt, F.-E. Legiret, A. D. Postle, and E. P. Achterberg. 2013. Nutrient enrichment can increase the susceptibility of reef corals to bleaching. Nat. Clim. Change **3**: 160–164. doi:10.1038/nclimate1661

Wiedenmann, J., and others. 2023. Reef-building corals farm and feed on their photosynthetic symbionts. Nature **620**: 1018–1024. doi:10.1038/s41586-023-06442-5

Wright, P. A. 1995. Nitrogen excretion: Three end products, many physiological roles. J. Exp. Biol. **198**: 273–281. doi:10.1242/jeb.198.2.273

Zhou, M., J. Granger, and B. X. Chang. 2022. Influence of sample volume on nitrate N and O isotope ratio analyses with the denitrifier method. Rapid Commun. Mass. Spectrom. **36**: e9224. doi:10.1002/rcm.9224

Conflict of Interest

No conflict of interests declared.